Pure Appl. Geophys. 173 (2016), 3757–3774
© 2016 Springer International Publishing
DOI 10.1007/s00024-016-1410-0

Pure and Applied Geophysics

Probabilistic Hazard of Tsunamis Generated by Submarine Landslides in the Cook Strait Canyon (New Zealand)

Emily M. Lane,[1] Joshu J. Mountjoy,[2] William L. Power,[3] and Christof Mueller[3]

Abstract—Cook Strait Canyon is a submarine canyon that lies within ten kilometres of Wellington, the capital city of New Zealand. The canyon walls are covered with scars from previous landslides which could have caused local tsunamis. Palaeotsunami evidence also points to past tsunamis in the Wellington region. Furthermore, the canyon's location in Cook Strait means that there is inhabited land in the path of both forward- and backward-propagating waves. Tsunamis induced by these submarine landslides pose hazard to coastal communities and infrastructure but major events are very uncommon and the historical record is not extensive enough to quantify this hazard. The combination of infrequent but potentially very consequential events makes realistic assessment of the hazard challenging. However, information on both magnitude and frequency is very important for land use planning and civil defence purposes. We use a multidisciplinary approach bringing together geological information with modelling to construct a Probabilistic Tsunami Hazard Assessment of submarine landslide-generated tsunami. Although there are many simplifying assumptions used in this assessment, it suggests that the Cook Strait open coast is exposed to considerable hazard due to submarine landslide-generated tsunamis. We emphasise the uncertainties involved and present opportunities for future research.

Key words: Probabilistic, tsunami, submarine landslides, Cook Strait.

1. Introduction

While submarine earthquakes are the most common cause of tsunamis, tsunamis can be generated by a range of geological processes including submarine landslides. This has been clearly demonstrated over the last century by several major events including the Grand Banks submarine failure of 1929 that caused a tsunami which killed 28 people (Fine et al. 2005), and the 1997 Papua New Guinea tsunami that caused water elevations greater than 12 metres in Sissano Lagoon and killed over 2000 people (Tappin et al. 2008). While both these events were also associated with an earthquake, in both cases it was the submarine failure that is thought to have initiated the bulk of the tsunami energy (Fine et al. 2005; Tappin et al. 2008). There is speculation that other co-seismic tsunamis may have also been augmented by landslides triggered by the earthquakes (Kawamura et al. 2014), including the 2011 Tohoku-oki tsunami (Strasser et al. 2013; Tappin et al. 2014). Submarine landslide-generated tsunamis (SLT) can pose a significant threat in some locations—especially in areas where the edge of the continental shelf is incised close to the land. SLT can also cause a tsunami hazard in places where co-seismic tsunamis are unlikely (Grilli et al. 2009). SLT typically have a different pattern of impact than earthquake-generated tsunamis, tending to be strongly concentrated over a relatively small length of coast with more limited propagation into the far-field (Harbitz et al. 2006; Ma et al. 2013; Okal 2003; Okal and Synolakis 2003, 2004). However, large-volume submarine landslides, e.g. the Storegga slide or the Currituck slide, can present long run-out and substantial regional impact (Bondevik et al. 2005; Geist et al. 2009; Løvholt et al. 2015).

Generally, SLT have been left out of probabilistic tsunami hazard assessments (PTHA) (Gonzalez et al. 2009; Leonard et al. 2014) because they are difficult to assess. As they are a localised phenomenon, far more scenarios may need to be considered in order to obtain a comprehensive assessment of the hazard

[1] NIWA, PO Box 8602, Riccarton, Christchurch 8011, New Zealand. E-mail: Emily.Lane@niwa.co.nz
[2] NIWA, Private Bag 14901, Kilbirnie, Wellington 6241, New Zealand.
[3] GNS Science, PO Box 30-368, Lower Hutt 5040, New Zealand.

Reprinted from the journal

(Harbitz et al. 2014) and the epistemic uncertainties in hazard analyses will consequently tend to be greater. Full three-dimensional modelling of the water and landslide with specified rheology is very computationally demanding (Abadie et al. 2012; Gisler et al. 2006; Liu et al. 2005). While some procedures for modelling tsunami initiation exist (e.g. TOPICS: (Enet and Grilli 2007; Enet et al. 2003; Watts et al. 2003, 2005), Two-layer models (Imran et al. 2001; Savage and Hutter 1989; Voellmy 1955) or prescribed bottom motion with a Kajiura Filter (Kajiura 1963), see also Løvholt et al. (2015) and references therein), these are not as well established as the use of Okada (1985) for co-seismic tsunami initialisation.

More recently, PTHAs have started to include the hazard due to submarine landslides, particularly in places where the co-seismic hazard is relatively low and so SLT represent the most likely tsunami scenario (Geist and ten Brink 2012; Geist and Lynett 2014; Grezio et al. 2012; Grilli et al. 2009; Pampell-Manis et al. 2016). These have used either a Monte Carlo Simulation approach or a Bayesian approach (Grezio et al. 2010, 2012). In the case of the Monte Carlo simulation approach, a simple rule of thumb is typically used to approximate the tsunami height at the coast in order to calculate the large number of simulations needed. Other hazard assessments have also considered SLT and given estimates of likely sizes and recurrence intervals (ten Brink et al. 2006, 2009, 2014).

Wellington, the capital city of New Zealand, lies in a harbour on the south end of the North Island of New Zealand (see Fig. 1). It sits astride the boundary between the Indo-Australian Plate and the Pacific Plate. The mouth of Wellington Harbour opens into Cook Strait, a narrow stretch of sea lying between the two main islands of New Zealand. On the eastern side of Cook Strait a submarine canyon, Cook Strait Canyon, incises close to shore. The side walls of the Cook Strait Canyon show evidence of many landslides ranging in size from 0.1 km^3 to just over 1 km^3—large enough to cause a considerable local tsunami. The head of Nicholson Canyon, a tributary of Cook Strait Canyon, lies within 10 km of Wellington.

The shores of Cook Strait show evidence of past tsunamis. Intact whale skeletons were discovered over 40 m above sea level on the Miramar peninsula at the opening to the Wellington harbour (Anonymous 1908), for which a tsunami is a possible explanation (Goff and Chague-Goff 2009). Evidence for palaeotsunamis has also been discovered on the Wairau Bar just south of Blenheim on South Island (Goff and Chague-Goff 2012; Goff et al. 2010; King and Goff 2010; McFadgen and Goff 2007), and at Big Lagoon nearby (Clark et al. 2015). While the sources of these paleotsunamis are generally either not known or only weakly constrained, it is clear from the historical record that the Wellington region faces considerable hazard from earthquake-caused tsunamis. For example, in 1855 a magnitude 8.2 earthquake shook the then recently founded settlement of Wellington. The tsunami generated by this earthquake overtopped the Rongotai Isthmus and caused waves that reached over 10 m high in the Wairarapa (Downes 2014). The Cook Strait sea floor is riddled with numerous faults and while some of these are tsunamigenic, many are strike slip and would not be expected to cause tsunamis directly. They could, however, trigger submarine landslides, thus in order to fully understand the tsunami hazard facing Wellington we need to be able to incorporate the SLT hazard into a full PTHA of the region.

2. *Method*

We wish to perform a PTHA due to SLTs in terms of the annual probability of a given maximum water elevation at coast, occurring at locations on a contour around the Cook Strait coastline (Wellington and Wairarapa in the North Island and Blenheim, Marlborough in the South Island) (Fig. 1). To achieve this, we bring together different strands of information as shown in Fig. 2. We need to understand the geology of landslides within the Cook Strait Canyon and use this information to develop an empirical magnitude/frequency relationship for landslide occurrence. An outline of how this is estimated is given in Sect. 2.1. In parallel with the geological research, we must understand the effect of the landslide on the ensuing tsunami. Specifically, we wish to know the size of the

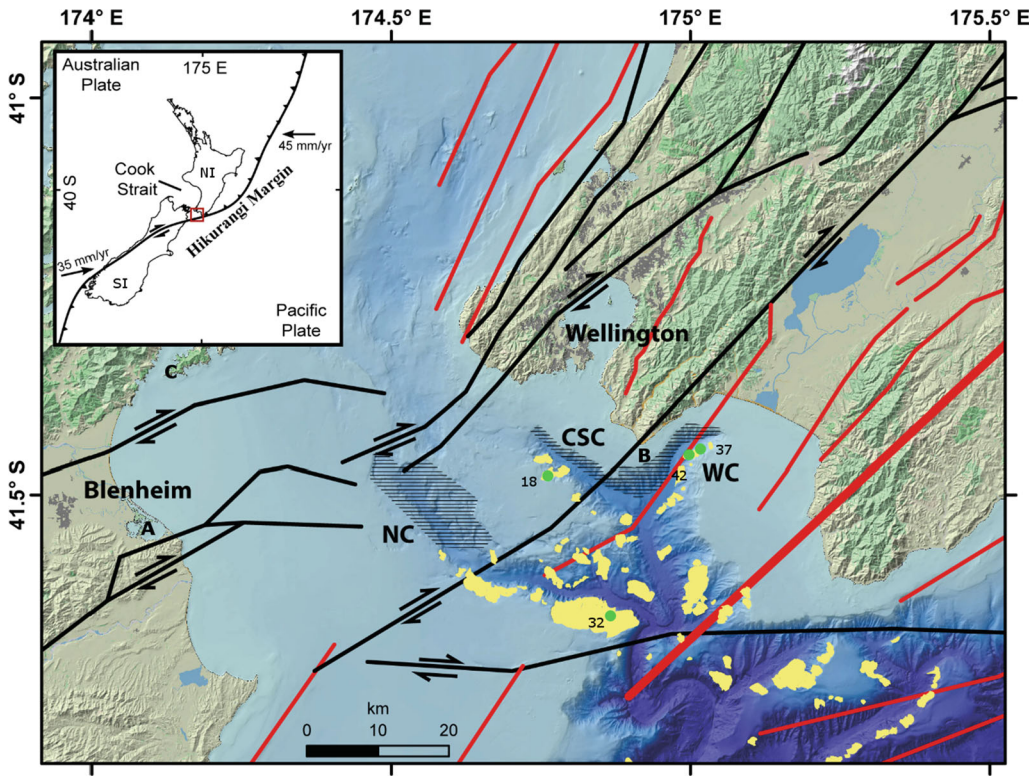

Figure 1
Location and setting. *Inset* shows location of Cook Strait study area in the context of the active plate boundary. Plate motion from Beavan et al. (2002). The North and South Islands are labelled NI and SI, respectively. Main figure shows the Cook Strait Canyons bathymetry with Nicholson Canyon (NC), Cook Strait Canyon (CSC), Wairarapa Canyon (WC). *Yellow polygons* are mapped landslides after Micallef et al. (2012). Black hatching indicates areas where recent geomorphic processes obscure landslide scars. *Line segments* are earthquake sources from the National Seismic Hazard Model (after Stirling et al. 2012) with strike slip faults (*black*) and reverse faults (*red*), and the plate boundary thrust in *bold red*. Green dots show locations of Core ID samples used in Table 1. *A* shows the location of the Wairau Bar, *B* Turakirae Head and *C* Marlborough sounds

tsunami (using maximum water elevation at the coast as the hazard impact measure) generated by a landslide of a given size and source location within the canyon. We achieve this through modelling (as documented in Sect. 2.2). Finally, we combine this information to get the PTHA (Sect. 2.3).

2.1. *Submarine Landslide Magnitude–Frequency Relationship*

An empirical magnitude/frequency relationship has been developed based on previous analysis of the distribution and age of landslides within the Cook Strait canyon system (Micallef et al. 2012; Mountjoy et al. 2009, 2014). A regression of the landslide volume distribution presented in (Micallef et al. 2012) provides a magnitude distribution and, when plotted against the area, confirms that the landslides within the canyon can be classified as deep seated (Fig. 1). In this study, we choose to focus on the landslides within the upper canyons (Nicholson Canyon, Cook Strait Canyon and Wairarapa Canyon in Fig. 1) as the landslides in the down-canyon region beyond this are in much deeper water (>650 m) and further from populated areas and, therefore, considered less likely to pose a hazard. Should any of these down-canyon landslides prove to be tsunami-genic, it would be in addition to the tsunami hazard calculated here.

Landslides within the upper canyons are not clearly clustered in any way but are relatively evenly distributed. A caveat to this is that landslide features

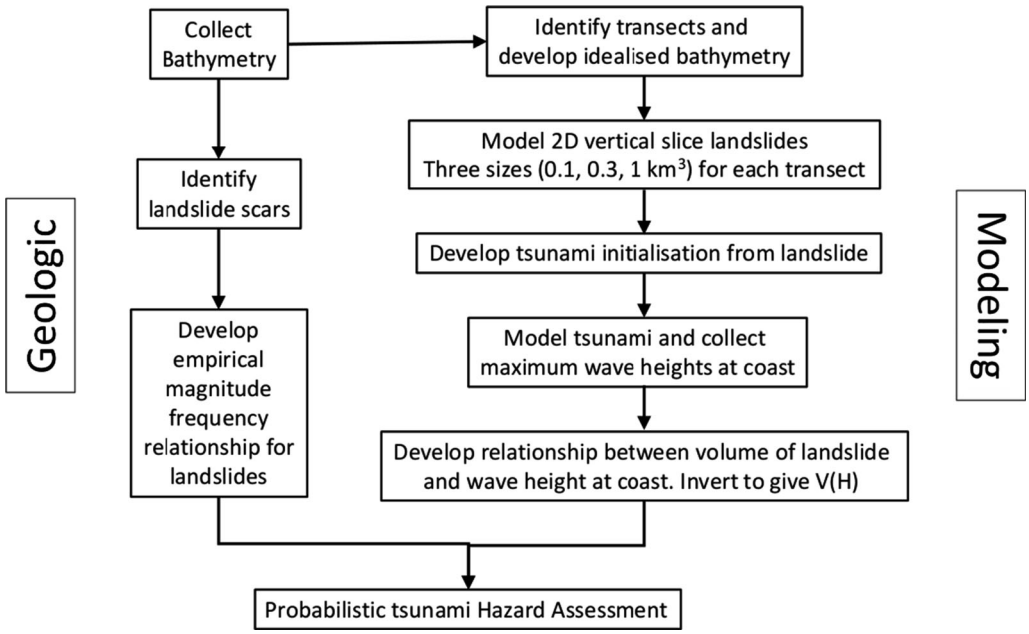

Figure 2
Flow diagram of probabilistic tsunami hazard assessment

are obscured in the head regions of the canyons (hatched areas in Fig. 1). In the upper arm of Cook Strait Canyon, the geomorphology is altered by erosion and deposition related to vigorous tidal currents (Mountjoy et al. 2014; Proctor and Carter 1989). On the northern walls of Nicholson and Wairarapa canyons, the exposed Greywacke bedrock is steep and heavily gullied, and though past mass failures are inferred no evidence for these remains (Mountjoy et al. 2009). We infer that the same distribution of failures has occurred in the ~25 % of the canyon where the evidence for landslides is obscured.

We chose to employ a volume statistics approach as this best fits our dataset. While we do have a limited amount of geotechnical data (e.g. Mountjoy et al. 2014; Mueller et al. 2016), we do not have anywhere near adequate coverage to characterise the geotechnical variability within the canyon walls (c.f Grilli et al. 2009). We use the extrapolated landslide population to determine the number of landslides for each volume bin from which we derive the number of landslides greater than or equal to a given volume. A regression model was then fitted to these data to produce an equation for the expected number of landslides of at least volume *V*, over the entire time period, viz.

$$p_{\text{Cook Strait}}(v > V) = 3.28V^{-1.53} \quad (1)$$

where *p* stands for probability, i.e. in this case it is the probability within Cook Strait that the landslide volume is greater than *V*. Geophysical data and geological samples were collected in 2011 during the *RV Tangaroa* voyage Tan1103 (Mountjoy et al. 2014). A key objective of TAN1103 was to collect data to constrain the age of several landslides. Evidence for landslides is represented in the canyons by evacuated failure scars (head scarps, lateral scarps and failure planes) that indicate deep-seated bedrock failures as supported by the volume vs area plot in Fig. 1 of Micallef et al. (2012) showing an exponent of 1.3. This suggests that the landslide mechanism is most likely to be translational block sliding (Micallef et al. 2012). No landslide deposits are preserved on the seafloor of the upper Cook Strait canyons associated with canyon wall failure. This indicates that landslides are disintegrative as material must substantially break up to be completely smothered or

Table 1

Landslide dating data

Core ID	Date depth (m)	C14 date (years BP)	Cover depth	Landslide age (years BP)
Stn 18	1.8	14,217 ± 127	NA	14,217 ± 127[a]
Stn 32	2.7	1031 ± 85	6.96 ± 0.2 m	2658 ± 295
Stn 37	2.5	159 ± 79	3.2 ± 0.2 m	204 ± 125
Stn 42	2.4	1470 ± 75	5.84 ± 0.2 m	3090 ± 486

Core sites are shown in Fig. 1

[a] The calibrated age is for benthic forams found at the base of the core from sea level low-stand, which agrees with relict shell hash material observed in core. This age is applied to the landslide scar with no assumption of accumulation rate

alternatively deposits are rapidly removed by strong canyon currents (Mountjoy et al. 2014). Geological data for dating landslides were collected by coring within canyon wall landslide scars (Table 1, core locations shown in Fig. 1). Using carbon-14 (^{14}C) radiometric dating of benthic foraminifera found at the base of the cores, we derived local sedimentation rates and extrapolated these down to the landslide failure plane imaged on sub-bottom profiler data. It is acknowledged that the sedimentation rates in the canyons are highly variable and this has been discussed in more detail by Mountjoy et al. (2014); however, with the availability of only one date per core we assume a simple linear sedimentation rate. We determined the age for four of the landslides as between 200 and 14,000 years BP.

As we cannot collect age control data for all the landslides within the canyon to get frequency information, we have taken the approach of inferring an age for the canyon landscape based on large-scale environmental changes documented in the area. During sea level low-stand periods (i.e. during the last ice age c. 20,000 years BP), the erosion and sediment deposition within most global canyon systems were dramatically enhanced. We expect this to also be true for the Cook Strait Canyons (Lewis et al. 1994; Mountjoy et al. 2009). We infer that the geomorphic evidence for landslides observed in the canyons post-dates the start of sea level rise (i.e. the start of the current interglacial period) as this is inferred to have coincided with a dramatic reduction in canyon forming downslope sediment processes. We infer a maximum time period for the occurrence of the landslide population of 20,000 years. The present day shoreline, oceanographic and climatic regime was achieved in the early Holocene (c. 10,000 years BP) and this may be a lower bound for the landslide age population. Indeed, one of the dated landslides occurred prior to this date. During the sea level low-stand, a land bridge formed between the northwestern South Island and Taranaki, creating a large tidal embayment through Cook Strait (Lewis et al. 1994; Proctor and Carter 1989). This land bridge breached approximately 15,000 years BP as sea level rise initiated, likely releasing a large amount of sediment resulting in a short period of intense down-canyon sediment transport. We infer that this breach of the landbridge and subsequent enhanced activity would be the most likely point in time to define the "clock-reset" for Cook Strait Canyon landslides. The landslide ages presented in Table 1 all fall within this time period which supports this hypothesis. Our age model for the mapped landslide population is, therefore, 15 ± 5 kyrs. Although it is unlikely that the landslide events are evenly distributed through this time period, we have no data to base an alternative time varying model and so make the simplified assumption of a Poissonian distribution.

To derive an overall magnitude/frequency relationship for landslide occurrence in the canyons, we divide Eq. (1) by the inferred time period over which they occurred. That is, the annual probability of getting a landslide of minimum size V somewhere in the upper Cook Strait Canyon is:

$$p(v > V) = \frac{1}{\tau} = \frac{3.28V^{-1.53}}{15,000} \qquad (2)$$

Figure 3 shows this equation in purple. Also shown on the grid is how the equation changes if the

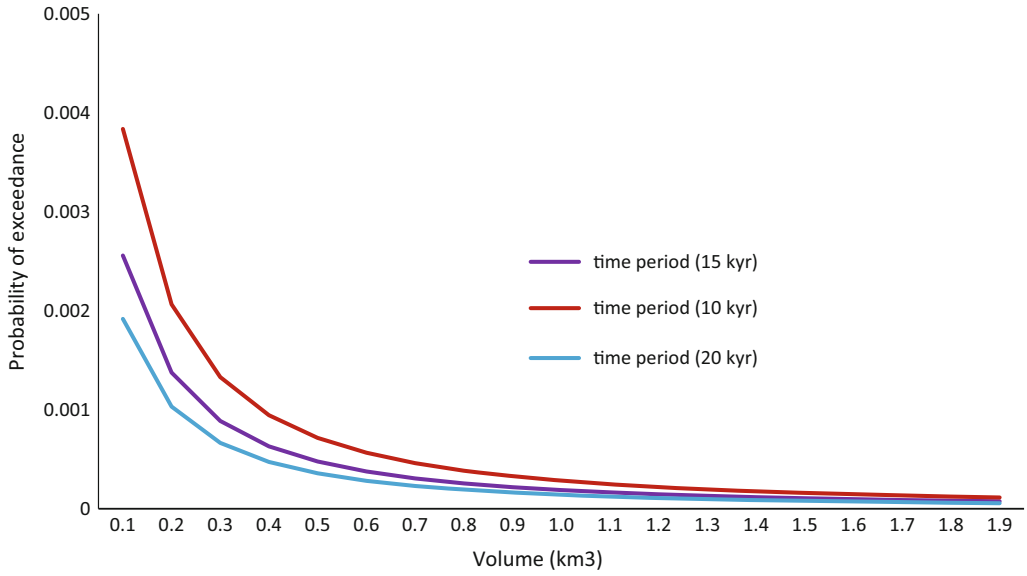

Figure 3
Landslide magnitude–frequency *curve* for Cook Strait Canyons

time period over which the landslides occurred is as short as 10,000 years (red) or as long as 20,000 years (blue).

If we divide the canyon up into n_y separate regions (which in this case will be the 176 transects as discussed in the next section) and, in the absence of any data to the contrary, assume that this probability is equally distributed across these regions, then the annual probability of a landslide of volume $>V$ occurring in region y is:

$$p_y(v > V) = \frac{3.28V^{-1.53}}{n_y 15,000} \tag{3}$$

If some regions are more likely than others to initiate landslides, this information could be taken into account by adjusting the probability by

$$p_y(v > V) = w(y)\frac{3.28V^{-1.53}}{15,000} \tag{4}$$

where $\sum_y w(y) = 1$. This still assumes that the overall magnitude–frequency relationship holds over the canyon as a whole. That is, while some areas might be more prone to landslides, in general the proportion of larger to smaller landslides is still the same (e.g. there are no areas that are only prone to smaller landslides). However, for the present work we do not have enough information to differentiate between the landslide hazard in different regions so, at this stage, we assume it is equal everywhere (i.e. through use of Eq. 3 for this analysis).

2.2. *Landslide and Tsunami Modelling*

The next step in the PTHA is understanding the effect of the SLT of a certain volume occurring at a given location. We achieve this through modelling possible events. The modelling is done using Gerris, a highly flexible open source fluid flow solver framework for both two and three dimensions based on an adaptive quadtree (oct-tree in three dimensions) (Popinet 2003). Gerris is able to solve a range of different fluid flow equations and has been used to model many different fluid flow phenomena including multiphase flows (using the Volume of Fluid (VoF) functionality (Agbaglah et al. 2011), ocean currents (Popinet and Rickard 2007) and tsunamis (Popinet 2011, 2012) (using the Saint–Venant solver—nonlinear shallow water equations). This allowed us to model both the tsunami initialisation from the landslide and the tsunami propagation with the same package. We used Gerris' VoF capabilities with three phases (landslide, water and air) for

modelling the initialisation of the tsunami by the landslide and the Saint–Venant solver (equivalent to solving the shallow water equations) to model the tsunami to the shoreline once it was initiated. We discuss the details of the modelling later in this section. For a recent overview of other submarine landslide numerical modelling methods, please see Løvholt et al. (2015).

SLT are localised events and, especially in the case of landslides occurring in Cook Strait Canyon, the details of the source location significantly affect the ensuing tsunami. This is because different locations in Cook Strait canyon direct the landslide towards, away from or parallel to the coast, they have very different slope angles—both for the sliding side and the opposite wall and they also have different bottom depths. Additionally, bathymetry and coastline can either shelter or focus the wave energy towards different locations.

Our first step to account for this variation was to divide the canyon into transects. These transects represent the range of possible source locations for landslides within the upper canyon. To capture the variation, transects were spaced approximately 1 km apart as shown on the left hand side of Fig. 4. At each transect location, an idealised bathymetry was extracted from the cross-sectional bathymetry at that transect. The bathymetry represents the transect as a flat shelf, a down slope, a (possibly sloping) bottom, a far wall and flat far shelf. The location of the transect and its direction across the canyon was also stored. Figure 4 (right-hand side) shows an example of the two-dimensional idealised bathymetry for transect 64 with the green showing a vertical representation of the 0.1 km^3 volume landslide.

For each transect, three landslides sizes were modelled, 0.1, 0.3 and 1 km^3 which represent a small, medium and large landslide given the range of landslide sizes seen within the canyon. At a later stage in the PTHA analysis (Sect. 2.3), curve fitting is used to provide approximate results for landslides with volumes other than at these data points; the accuracy of the results could be improved by adding further data points for other volumes of landslide, which we leave for subsequent work. Altogether 528 scenarios were modelled, so it was important that the modelling process was efficient.

We assumed that the landslide initiates from the top of the canyon and its map view is square. Thus, the length of the landslide was chosen so that the desired volume lay within the right-angle prism with a square top. The only exception to this was for cases of large landslides where the landslide reached from the top of the canyon to the bottom without the desired volume being obtained. In these cases, the length of the landslide was fixed as being the horizontal distance from the head to the foot of the canyon and the width of the canyon was adjusted in order to achieve the desired volume. This change in width does not affect the 2D vertical slice modelling used to model the landslide process but it does affect the conversion from the 2D vertical slice model to the

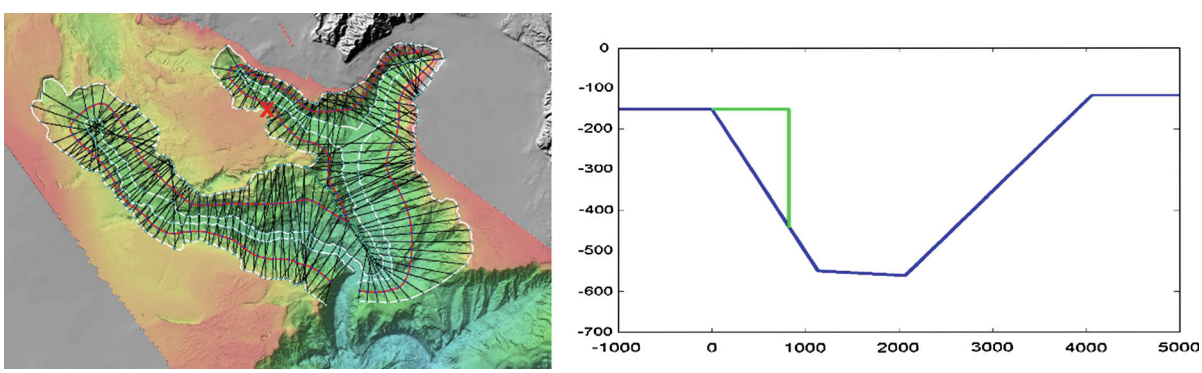

Figure 4
LHS Upper Cook Strait Canyon with 176 defined transects in total. *RHS blue line* shows the idealised two-dimensional vertical representation of transect 64 (located at *red* x on LHS); *green line* shows the idealised landslide

2D horizontal model used for modelling tsunami propagation, with the resulting wave being higher and wider in the transverse direction.

We modelled the landslides using a VoF approach similar to Abadie et al. (2012), where the slides were represented as dense, semi-rigid fluids, with air and water also modelled as fluids with different densities. In our modelling, the descending landslide was treated as a rigid block until the toe of the block reaches the canyon floor, at which point it is modelled as a dense fluid with no internal rigidity. These assumptions are approximations to our assumed picture of the true situation in which some deformation of the landslide volume is expected to occur during descent, and conversely complete breakup of the landslide mass into a dense fluid does not occur at the bottom of the slope. The dynamics of the descending block, and of the dense fluid motion on reaching the bottom, are part of the equations of motion solved by Gerris, i.e. there is no external imposition of the kinematics. To maintain a solid descending block within the fluid-dynamics solver, the velocity of each 'fluid' element in the landslide was reset to match the overall centre-of-mass velocity for the whole descending block at each timestep; this ensures that the block retains its shape. 3D modelling was possible but very computationally expensive and it was not feasible for the number of simulations required. After comparing 3D modelling where the landslide had a finite width with 2D vertical slice modelling, we decided to use 2D vertical slice modelling for the landslide scenarios and then use an approximation to transform the water level taken from that into a 2D horizontal surface. This was then used as the initial condition for the tsunami modelling. Lane et al. (2016) documents the conversion from the 2D vertical slice landslide modelling to the initial condition for the tsunami propagation modelling which takes place in the horizontal plane. Once we expanded the 1D water height distribution into a 2D water height surface, we also needed to rotate the surface so that the direction of the landslide matched that of the transect and to translate the initial condition so that it occurred at the correct source location within Cook Strait. Figure 5 shows the one-dimensional wave height as modelled in the two-dimensional vertical slice modelling for one example and also the two-dimensional plan view surface water elevation it is transformed into for use as an initial condition. Figure 6 shows the range of depths and slopes in the 176 transects (taken from the actual bathymetry) and also the initial accelerations and Froude numbers of the landslides as modelled using the above procedure.

Once we created the initial condition, we simulated the ensuing tsunami using the Saint–Venant equations (equivalent to the shallow water equations) over a 2 h simulation period with a maximum level of refinement for the adaptive grid of 100 m; that is to say that Gerris dynamically alters the grid resolution according to the scale of the simulated waves down to a minimum grid size of 100 m. For each scenario, i.e. each combination of source location and landslide size, we saved the maximum water elevation over the simulation at a contour of points along the Wellington and Blenheim/Marlborough coastline at a depth of 1 m. We used these results for the probabilistic modelling documented in the following subsection (results shown in Fig. 8 are on this contour of points).

Figure 7 shows the maximum water elevations over the simulation run for landslides of volume 1 km^3 for various source locations. This clearly shows that the differences in the configuration of the landslides and the bathymetry based on source location play a large role in the results obtained and vindicates our decision to model these scenarios separately. Proximity and the direction of the slide pointing towards land tend to give larger wave heights at the coast. Source locations where the canyon floor is deeper and there is a greater distance from top to bottom also give larger wave heights—especially in the direction of the landslide. Wave focussing is also important as can be seen in the top two right-hand side scenarios which have sources in the eastern Wairarapa Canyon, which is further from Wellington. The top right-hand side scenario shows the energy being refracted around towards Wellington. Wellington is less exposed to landslides initiating further north in the canyon because it is sheltered by Turakirae Heads. In the middle right-hand side scenario, the topography channels the tsunami energy into two main beams, one wraps around, hitting the North Island to the west of Wellington and the other is guided towards the South Island.

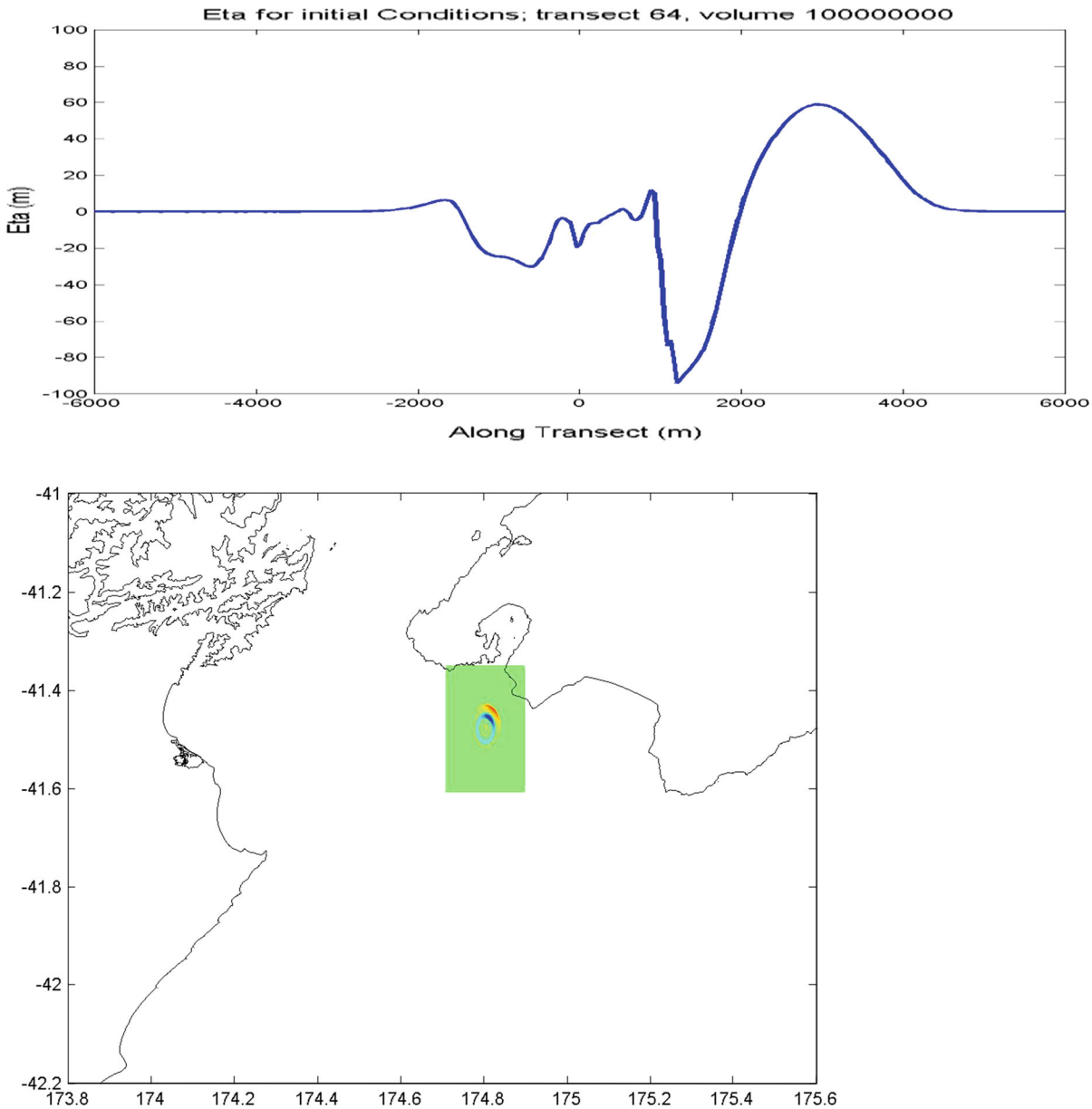

Figure 5
Top Water elevation at end of simulation for one scenario. *Bottom* 1D Water level expanded to 2D surface, rotated to correct direction and shifted to source location for use as initial condition

2.3. *Probability*

This subsection brings together the two strands of research: the magnitude–frequency relationship of the landslides within the canyon developed in Sect. 2.1 and the numerical modelling which describes the effect of the landslide in terms of the maximum water elevation at the coast of the tsunami that the landslide could generate developed in Sect. 2.2.

Consider a set of points of interest x (in this case the contour around the Cook Strait coastline), where we wish to calculate the annual probability of a tsunami with maximum water elevation exceeding h for each point in that set. The hazard comes from

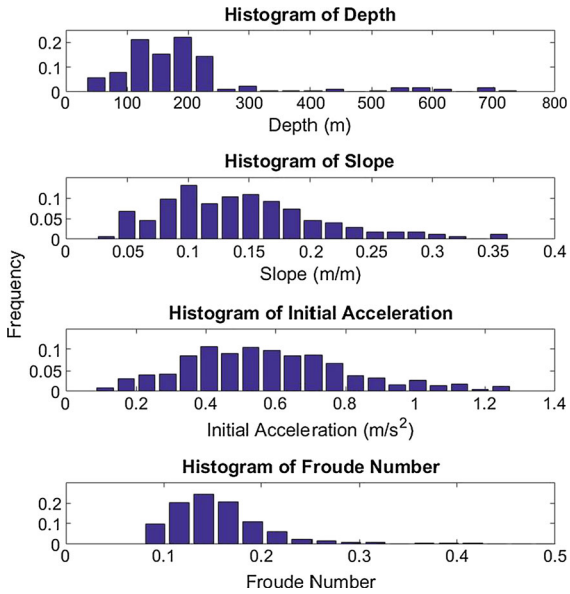

Figure 6
Histograms showing the depths of the top of the landslide, the slopes of the sliding surface (taken from the actual bathymetry at the transect locations) and the initial accelerations and Froude numbers of the landslides (as calculated from measurements taken during the modelling)

landslides on the set of source locations which we denote y. We wish to know the maximum tsunami wave elevation at x, caused by a landslide of volume v, initiated at a location y, this can be written as $H(x, y, V)$.

We simulated tsunamis for three landslide volumes (0.1, 0.3 and 1 km^3) for each of the 176 transects. This gives values for $H(x, y, 0.1)$, $H(x, y, 0.3)$ and $H(x, y, 1)$. Furthermore, we can assume that $H(x, y, 0) = 0$, i.e. if there is no landslide there will be no tsunami. We fitted a curve of the form:

$$H(x, y, V) = 10^{b(x,y)} V^{m(x,y)} \tag{5}$$

Where $b(x,y)$ and $m(x,y)$ are determined by the curve fitting. We then inverted Eq. (5) to get the volume of landslide required on transect y to produce a tsunami with maximum water elevation, H, at point x

$$V(x, y, H) = \left(\frac{H}{10^{b(x,y)}}\right)^{1/m(x,y)} \tag{6}$$

By combining Eq. (6) with Eq. (3), the annual probability of there being a landslide of a given size

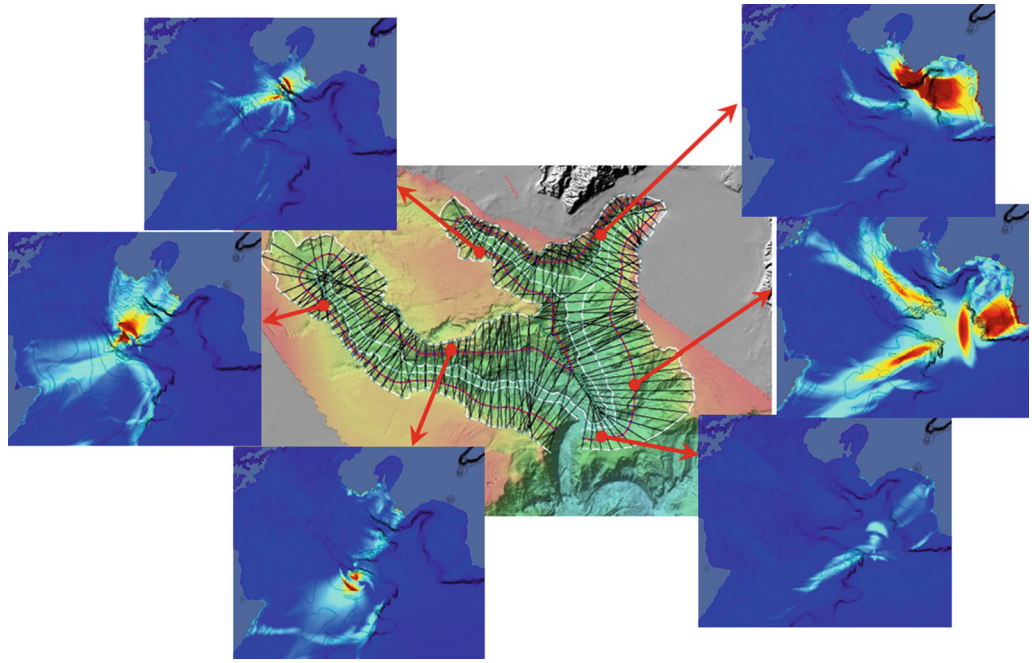

Figure 7
Maximum water elevations for landslides of volume 1 km^3 originating in different parts of the canyon. *Red dots* indicate the source location of the forcing landslide. The variety of results vindicates our decision to separately model each of these scenarios. *Colours* range from zero (*dark blue*) to ten metres (*dark red*)

on a given transect, we calculated the annual probability of a tsunami originating at transect y, causing maximum water elevation greater than H, at point x, viz.,

$$p_y(h(x) > H) = \frac{3.28V(x,y,H)^{-1.53}}{n_y 15,000} \quad (7)$$

We then summed over all the possible source locations and calculated the overall annual probability of a tsunami caused by a submarine landslide creating a maximum water elevation greater than H at point x as:

$$\Pr(h_{\max}(x) > h) = \sum_y \frac{3.28V(x,y,h)^{-1.53}}{n_y 15,000} \quad (8)$$

If we are interested in the tsunami hazard over a region rather than at a specific point we can calculate this using a similar formula to Eq. (8) but minimising the volume over all the sites of interest (e.g. x in a region X_0) before continuing with the calculation (i.e. the probability that somewhere within the coastal region X_0 an SLT causes a maximum water elevation greater than h):

$$\Pr(h_{\max}(X_0) > h) = \sum_y \frac{3.28\left(\min_{x \in X_0} V(x,y,h)\right)^{-1.53}}{n_y 15,000} \quad (9)$$

We must calculate the probability in this combined way as the probabilities at neighbouring sites of interest will not be independent.

When summing the probabilities over the transects, we set a cutoff on the probability based on a volume of 0.1 km^3—the smallest bin size in the histogram of landslide sizes. If the volume was less than this, we set the probability to that for a volume of 0.1 km^3. Because of the equation used, the probability of occurrence asymptotes as the volume goes to zero. With the curve fitting, sometimes moderate maximum water elevations can be caused by unrealistically small landslides. This in conjunction with the probability of small landslides being very high can skew the results.

We also excluded from the analysis any site/transect combination where at least one of the maximum water elevations is zero or less than 10^{-4} m or where the curved fitted was flat or not increasing (i.e. $m(x,y) < 0.01$). This removed 2276 site/transect pairs which represent 1.79 % of the total number of combinations and so is not expected to significantly affect the results. We did not set an upper cutoff for landslide volumes, which could affect the larger, low probability events, especially in places where the overall hazard is lower, but a slide larger than 2 km^3 is only expected once every 13,000 years on average (as calculated by Eq. 2).

Further details on the implicit assumptions made in these probabilistic calculations are discussed in greater detail in Sect. 4.

3. Probabilistic Tsunami Hazard Assessment

Figure 8 gives the estimated annual probabilities of wave elevations caused by SLT exceeding 5 m and 10 m at the selected coastal contour. The exposed southern coast of the North Island can clearly be seen to have the greatest hazard from SLT. Much of this coast has an annual probability over 1:2000 of a wave greater than 5 m at the coast. Around Turakirae Head, a wave greater than 10 m has an annual probability over 1:4000 with most of the rest of the North Island open coast having an annual probability of 10 m waves between 1:10,000 and 1:20,000. The region with the next greatest hazard is the open coast of Marlborough Sounds which shows only a slightly lower level of hazard but is generally less populated than the Wellington coast. Much of the region in the South Island south of the Wairau Bar also shows that a 5 m wave could be expected every five to ten thousand years. Waves greater than 10 m could be expected every few thousand years. Locations in enclosed bays and harbours like Wellington Harbour and the inner Marlborough Sounds have considerably reduced hazard with large waves being unlikely to make it far into these regions.

Because of the local nature of SLT, a large wave in one area of Cook Strait does not necessarily mean it will happen over the entire region. Another consequence of this is that the annual probability of a certain maximum water elevation occurring some-

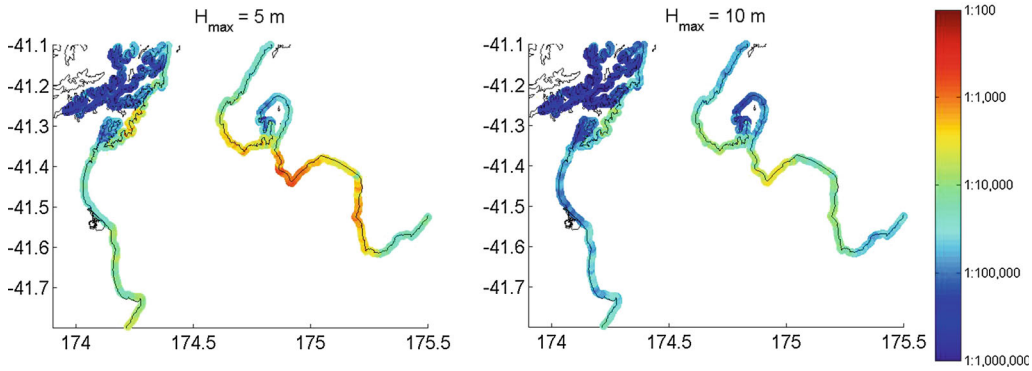

Figure 8
Hazard results as probability of exceedance for 5 m and 10 m maximum water elevations for coastal sites of interest around Cook Strait. Scale shows exponential value for annual probability of exceedance (i.e. 10^{-2}–10^{-6})

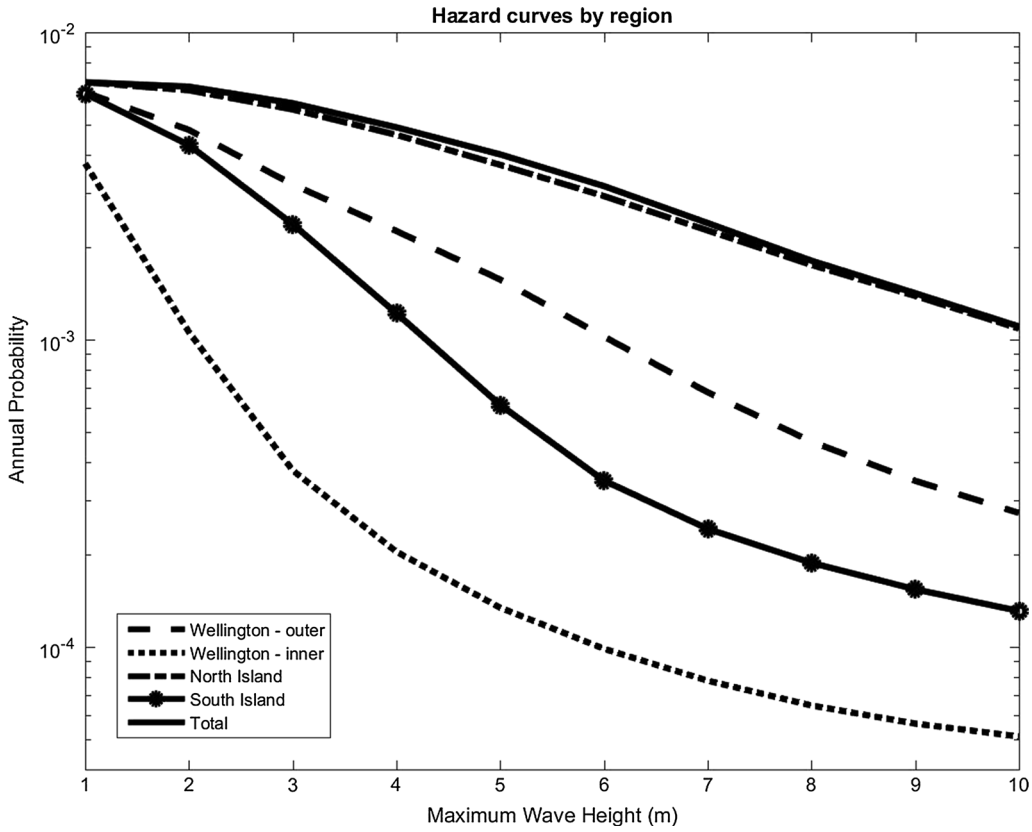

Figure 9
Annual exceedance curves by region. Each shows the annual probability of achieving a maximum water elevation at coast over that level somewhere on that coastline. Wellington—outer and inner refer to the outer exposed coast and inner Wellington Harbour, respectively

where in a given region will be higher than the probability of it happening at any given location in that region. We also consider combined probabilities of a maximum water elevation exceedance over a given region (Fig. 9). Over the entire Cook Strait region, the annual probability of getting a maximum

water elevation at coast in excess of 1 m is around 1 in 150 years. From Eq. (2), this is equivalent to the annual probability of a landslide of size 0.1 km^3 somewhere in the Cook Strait Canyon. As expected, the likelihood of this occurring on the southern coast of the North Island is very high with its exceedance curve being almost equal to the total curve. The North Island curve and the total curve are almost exactly the same for maximum water elevations at coast of 1 m and 10 m with only minor differences for maximum water elevations between these. Thus, a big (>10 m) wave would be much more likely to occur on the North Island than the South Island. The probability of getting a maximum water elevation at coast over 5 m somewhere in the Cook Strait is still quite high at around 1 in 250 years. A maximum water elevation at coast over 10 m is expected to occur around every 900 years. Unfortunately, the paleotsunami data in this region are too sparse to provide any verification of this result. The probability of getting a maximum water elevation at coast of 1 m on the Wellington open coast and the South Island is very similar and only slightly lower than the overall probability. This is because many of the scenarios mapped could cause a tsunami of this size over several regions. The probability of larger waves falls off more rapidly on the South Island than it does for the exposed coast of Wellington. This is most likely because the South Island is further away from Cook Strait Canyon than the North Island and so the larger waves have dissipated somewhat as they travel over the continental shelf. Specific details of sources, wave focussing effects and dispersion could also play a role. Inside Wellington harbour, the probability of a maximum water elevation at coast greater than 1 m is around 1 in 270 years. The probability of larger waves falls off rapidly, with a maximum water elevation at coast of 3 metres having a return period of around 2500 years. These would most likely occur near the mouth of the harbour where it is more exposed.

4. Discussion and Uncertainties

This work shows that there is potentially a considerable hazard to the Cook Strait region due to SLT, especially on the open coast. In comparison with earthquake-generated tsunamis, the 1 in 2500 year expected maximum water elevation at coast hazard is also 10 metres (Power 2013). This is similar to the hazard due to SLT on the Wellington outer coast although the hazard within Wellington Harbour from SLT is considerably less. In addition, because co-seismic tsunamis tend to have longer periods and, therefore, have more time to inundate before withdrawal occurs, it is plausible that they are likely to inundate further inland for a similar maximum water elevation at coast, though we suggest further modelling is required to confirm this conclusion. The sequence of waves is also more likely to last longer: for these SLT, the majority of the energy occurs within the first few tens of minutes. Ideally, we would combine these SLT results with the earthquake-generated tsunami results to produce a PTHA from all sources. This could be achieved within a Bayesian Framework (Grezio et al. 2012). We would need to ensure a consistent hazard measure.

From a civil defence point of view, because landslides in Cook Strait Canyon are expected to be triggered by earthquakes, the local source evacuation recommendation, to self-evacuate in the event of strong or long duration shaking, stays the same (WREMO 2015).

Due to the multidisciplinary nature of this study, there are many uncertainties associated with the results. Here, we outline some of these uncertainties and possible ways of dealing with them. Our purpose in this study is to provide a framework for estimating the tsunami hazard, which can then be subsequently refined to explicitly include the various uncertainties in a quantitative way. We first consider the uncertainties in the results due to geological uncertainties and then we consider the uncertainties due to the modelling and inherent assumptions.

4.1. Geological Uncertainties

Determining the recurrence interval of submarine landslides using data from the source areas remains a very challenging topic. We know the general spatial and magnitude distribution of previous landslides but have had to infer an age period of 15 $\pm$ 5 kyr based on major landscape perturbations "resetting" the

canyon wall geomorphology. The uncertainty in this time period results in an adjustment of the probability of occurrence. Additionally, we have assumed that the landslide occurrence is a stationary process with the likelihood of landslide occurrence not changing over time. The effect of a non-stationary process would depend on the timescale of interest, but it would increase (decrease) the probability for a more (less) active period.

Another source of uncertainty is the possibility that several landslides could occur simultaneously, or a co-seismic tsunami could occur in conjunction with the SLT. Given that we expect the landslides to be triggered by nearby earthquakes, these are very real possibilities. Depending on the details of when they occur, the tsunamis might interact constructively at some locations, augmenting the maximum water elevation at coast, and (less often?) destructively at others; or the maximum water elevation at the coast of the combined events could be approximately the maximum over the two events. Exactly what would occur would very much depend on the details of the fault rupture and landslides, their source locations and the relative times that they occurred (as landslides are often delayed slightly compared with the main shock and can often be associated with one of the aftershocks—e.g. the 1997 Papua New Guinea tsunami (Tappin et al. 2008)). In the case where multiple landslide events may occur at the same time, the threshold for an event to occur would shift to a longer timeframe. This would affect the probability for smaller events. However, because we have used the empirical distribution of landslide sizes, this uncertainty would not affect the lower probability larger events as much.

Another simplification that we had to make was the assumption that landslides are equally likely throughout the entire canyon. While this is a reasonable starting point based on the relatively equal distribution of landslides throughout the canyon (i.e. we expect that all areas of the canyon have failed at some time), it is definitely a simplification. Because landslides within Cook Strait Canyon are expected to be triggered by seismic events, we could use seismic and geological information to identify areas that are more susceptible to landslides. Mueller et al. (2016) outline a process to calculate relative spatial susceptibility to landslides. This information could be accommodated within the current framework simply by assigning different weightings of probability to each of the source locations. A further step could be to assume a different magnitude–frequency relationship in different regions of the canyon (i.e. not just different weightings). In this case, these different relationships would need to be used for the different locations but the same overall methodology could be applied. Developing different magnitude–frequency relationships for different regions would require significant amounts of extra information, and it would still be necessary to ensure that the overall magnitude–frequency relationship agreed with that derived empirically. It is questionable whether enough information could be gathered to warrant this approach.

We also assume that the distribution of landslide occurrence is stationary over the period of interest (the current interglacial period) and that landslides do not have different likelihoods at different time. In that case, the probability would become dependent on whether or not we are in a geologically more active phase. There are only four dated landslide scars (Table 1), but their range is not inconsistent with a stationary distribution.

4.2. *Modelling uncertainty*

Because of the number of scenarios involved, we take a relatively simple approach to modelling the landslides: using a simplified landslide shape and bathymetry and a 2D vertical slice which assumes that the canyon extends unchanged in both directions and that the landslide cannot move laterally to the cross section of the canyon (e.g. once it hits the canyon bottom it cannot flow down the canyon). We also assume that the landslide fails as a cohesive mass and that it fails from the top of the canyon, both of which are conservative assumptions. We also assume that the landslide loses all rigidity on hitting the bottom of the canyon, becoming a dense fluid, and that the landslide dynamics and the coupled water motion arising from these assumptions are accurately modelled by the Gerris solver. Further approximations occur during the process of deriving a two-dimensional water surface that represents the water

disturbance generated by the landslide that is used to initialise the tsunami modelling.

Once we have finished the landslide vertical slice modelling and initialised the 2D plan view tsunami modelling, we assume that the vertical variation in the velocity is no longer important and that the St Venant equations are a reasonable approximation of the fluid motion. In reality, there will still be vertical variations in velocity. Future modelling using equations containing higher order approximations (such as the Boussinesq equations (Løvholt et al. 2013; Madsen et al. 2003; Pedersen 2008)) would be recommended to test this assumption, and if necessary to take these dispersive effects into account (Glimsdal et al. 2013).

Although there are many assumptions inherent in our modelling, it does allow the bathymetry of the canyon to shape the evolution of the landslide and ensuing tsunami. As such, and given that the results are amalgamated into a probabilistic hazard assessment, we suggest that this is a reasonable first step.

In addition, the process of developing this methodology and working through the case of Cook Strait identifies where the uncertainty lies in this endeavour and, therefore, highlights areas for future research to better understand both the processes and the hazard facing Wellington and the Cook Strait region.

The output from this hazard assessment is maximum water elevation at coast. If we were interested in inundation, it would also be necessary to take into account the aleatory uncertainty of the tidal level at the time of the tsunami. As Cook Strait is close to a tidal node, the tidal range is smaller than most of the rest of New Zealand at around 1 m (Walters et al. 2010) but will still have some affect. Various methods have been used to account for the tidal cycle in previous PTHAs (Adams et al. 2015; Lane et al. 2013).

Other PTHAs have used Monte Carlo Simulations to calculate the Probabilistic Tsunami Hazard Assessment (Grilli et al. 2009; Pampell-Manis et al. 2016). These have been able to take into account both the aleatory uncertainty within the simulation by picking source locations randomly and also the epistemic uncertainty by randomly selecting the simulation parameters from expert opinion selected distributions. The PTHA presented here models an ensemble of the possible landslides throughout the canyon. We are able to take into account the aleatory uncertainty of the size and location of the landslide by weighting the different ensemble members appropriately. However, this does not take the epistemic variation into account; a summary of epistemic uncertainties and the assumptions currently made regarding them is tabulated in Appendix 1.

5. Conclusions

We developed a methodology for assessing the probabilistic tsunami hazard due to submarine landslides in a submarine canyon with complex bathymetry. This method takes into account geological information about the distribution of landslide sizes and also the variations in the tsunami generated due to differences in the source location (strike, depth, canyon features, etc.) as well as the bathymetry and geography of the strait and the coast. Many of the assumptions implicit in the methodology indicate future areas where improvements to this probabilistic modelling could be made.

The application of this methodology to the case of the Cook Strait Canyon shows that tsunamis generated by submarine landslides are a hazard to the region—especially the open coast areas. This research shows that the hazard to the open coasts of the Wellington region is similar in some areas to that posed by co-seismic tsunamis (Power 2013), at least when considered in terms of maximum water elevation at coast. However, the actual inundation caused by the submarine landslides may be less because the shorter wavelength of the SLT means that it has less time available before withdrawal to run inland and inundate lower lying areas. Further research is recommended to incorporate the combined hazard from both co-seismic and SLT and to investigate the uncertainties outlined in the discussion section.

Acknowledgments

This work was supported by the New Zealand Natural Hazards Platform (Contracts 2012-NIW-03-NHRP

and CS-GNS-25) and by NIWA and GNS as part of its Government-funded, core research. The authors also wish to acknowledge the contribution of NeSI to the results of this research. New Zealand's national compute and analytics services and team are supported by the New Zealand eScience Infrastructure (NeSI) and funded jointly by NeSI's collaborator institutions and through the Ministry of Business, Innovation and Employment. URL http://www.nesi.org.nz. Thanks also to Finn Løvholt and an anonymous reviewer for their comments which have significantly improved this paper.

Appendix 1: Tabulation of uncertainties and corresponding assumptions

The purpose of this paper is to develop a first iteration probabilistic tsunami hazard model for landslide tsunamis in Cook Strait. This analysis contains many uncertainties, and rests on various assumptions and approximations that have been made. Before the conclusions of this report can form the basis for extensive mitigation measures, it will be important to thoroughly analyse the various uncertainties involved. This is a large and complicated task, and this paper is intended to provide only a starting point for such an analysis. In Table A.1, we summarise the various identified sources of uncertainty, and the assumptions we have made here with regard to them. Where we believe an assumption is conservative (biased towards a greater tsunami hazard) we have indicated this with a (+), where we believe that the assumption is optimistic (biased towards a lower tsunami hazard) we have indicated this with a (−), and where there appears to be no obvious bias we have indicated this with a (∼).

Table A.1: Tabulation of sources of uncertainty in the PTHA, and of assumptions made regarding them. Where it is thought that an assumption has a bias this is indicated with a (+) or (−) according to whether it is thought likely to increase or decrease the estimate of tsunami hazard. Where there is no clearly evident bias this is indicated with a (∼).

Uncertainty	Assumption
Accuracy of landslide magnitude–frequency distribution	Assessed survey data are representative of current day conditions (∼); un-assessed areas show the same M-F characteristics as the surveyed areas (∼); all scars were generated in rapid single-event landslides (+)
Position of landslide block on slope before failure	Top of slope (+)
Modelling assumptions on landslide rheology and failure mode—only one realisation modelled	Gerris Volume of Fluid solver used (∼)
Landslide density	Relative density of 2.0 (∼)
Shape of landslide body	Triangular prism (∼)
Degree of breakup of landslide block during descent	Block remains rigid and intact (+)
Degree of breakup of landslide material on hitting canyon floor	Total breakup into dense fluid (∼)
Inaccuracy in modelling caused by using simplified 2D vertical slice profile to represent 3D canyon shape	Simplified 2D profile approximates canyon with translational symmetry (∼)
Conversion of 1D water surface into initial condition for 2D tsunami propagation modelling	Accurate conversion of water levels (∼); water velocity at initiation of tsunami propagation model is zero (−), see Lane et al. (2016)
Effect of dispersion on tsunami propagation	Non-dispersive tsunami propagation equations (+)
Influence of bathymetry data quality	Used best available (∼)

References

Abadie, S. M., Harris, J. C., Grilli, S. T., & Fabre, R. (2012). Numerical modeling of tsunami waves generated by the flank collapse of the Cumbre Vieja Volcano (La Palma, Canary Islands): Tsunami source and near field effects. *Journal of Geophysical Research-Oceans*, *117*, C05030. doi:10.1029/2011JC007646.

Adams, L. M., LeVeque, R. J., & Gonzalez, F. I. (2015). The pattern method for incorporating tidal uncertainty into probabilistic tsunami hazard assessment (PTHA). *Natural Hazards, 76*(1), 19–39.

Agbaglah, G., Delaux, S., Fuster, D., Hoepffner, J., Josserand, C., Popinet, S., et al. (2011). Parallel simulation of multiphase flows using octree adaptivity and the volume-of-fluid method. *Comptes Rendus Méc, 339*(2–3), 194–207.

Anonymous (1908). Miramar relics, Evening Post, Vol. v. LXXVI issue 108: Wellington.

Beavan, J., Tregoning, P., Bevis, M., Kato, T., & Meertens, C. (2002) Motion and rigidity of the Pacific plate and implications for plate boundary deformation. *Journal of Geophysical Research-Solid Earth*, v. 107, no. B10.

Bondevik, S., Løvholt, F., Harbitz, C. B., Mangerud, J., Dawson, A., & Svendsen, J. I. (2005). The Storegga Slide tsunami comparing field observations with numerical simulations. *Marine and Petroleum Geology, 22*(1–2), 195–208.

Clark, K. J., Hayward, B. W., Cochran, U. A., Wallace, L. M., Power, W. L., & Sabaa, A. T. (2015). Evidence for Past Subduction Earthquakes at a Plate Boundary with Widespread Upper Plate Faulting: Southern Hikurangi Margin. *New Zealand: Bulletin of the Seismological Society of America, 105*(3), 1661–1690.

Downes, G. (2014) New Zealand Tsunami Database: Historical and Modern Records. http://data.gns.cri.nz/tsunami/. Accessed 17 May 2015.

Enet, F., & Grilli, S. T. (2007) Experimental study of tsunami generation by three-dimensional rigid underwater landslides. *Journal of Waterway Port Coastal and Ocean Engineering-ASCE 133*(6), 442–454.

Enet, F., Grilli, S. T., & Watts, P. (2003) Laboratory experiments for tsunamis generated by underwater landslide: comparison with numerical modeling. In Proceedings of the thirteenth (2003) International offshore and polar engineering conference (pp. 372–379).

Fine, I. V., Rabinovich, A. B., Bornhold, B. D., Thomson, R. E., & Kulikov, E. A. (2005). The Grand Banks landslide-generated tsunami of November 18, 1929: preliminary analysis and numerical modeling. *Marine Geology, 215*(1–2), 45–57.

Geist, E. L., & Lynett, P. J. (2014). Source Processes for the Probabilistic Assessment of Tsunami Hazards. *Oceanography, 27*(2), 86–93.

Geist, E. L., Lynett, P. J., & Chaytor, J. D. (2009). Hydrodynamic modeling of tsunamis from the Currituck landslide. *Marine Geology, 264*(1–2), 41–52.

Geist, E., & ten Brink, U. S. (2012) NRC/USGS Workshop Report: Landslide Tsunami Probability.

Gisler, G., Weaver, R., & Gittings, M. (2006). SAGE calculations of the tsunami threat from La Palma. *Science of Tsunami Hazards, 24*, 288–301.

Glimsdal, S., Pedersen, G. K., Harbitz, C. B., & Løvholt, F. (2013). Dispersion of tsunamis: does it really matter?. *Natural Hazards and Earth System Sciences, 13*(6), 1507–1526.

Goff, J. R., & Chague-Goff, C. (2009). Brief communication: cetaceans and tsunamis—whatever remains, however improbable, must be the truth? *Natural Hazards and Earth System Sciences*, v, *9*(3), 855–857.

Goff, J. R., & Chague-Goff, C. (2012). A review of palaeo-tsunamis for the Christchurch region, New Zealand, *Quaternary Science Reviews, 57*, 136–156.

Goff, J. R., Nichol, S., & Kennedy, D. M. (2010). Development of a palaeotsunami database for New Zealand. *Natural Hazards, 54*(2), 193–208.

Gonzalez, F. I., Geist, E. L., Jaffe, B., Kanoglu, U., Mofjeld, H., Synolakis, C. E., Titov, V. V., Arcas, D., Bellomo, D., Carlton, D., Horning, T., Johnson, J., Newman, J., Parsons, T., Peters, R., Peterson, C., Priest, G., Venturato, A., Weber, J., Wong, F., & Yalciner, A. (2009). Probabilistic tsunami hazard assessment at Seaside, Oregon, for near- and far-field seismic sources. *Journal of Geophysical Research-Oceans*, *114*, C11023. doi:10.1029/2008JC005132.

Grezio, A., Marzocchi, W., Sandri, L., & Gasparini, P. (2010). A Bayesian procedure for Probabilistic Tsunami Hazard Assessment. *Natural Hazards, 53*(1), 159–174.

Grezio, A., Sandri, L., Marzocchi, W., Argnani, A., Gasparini, P., & Selva, J. (2012). Probabilistic tsunami hazard assessment for Messina Strait Area (Sicily, Italy). *Natural Hazards, 64*(1), 329–358.

Grilli, S. T., Taylor, O.-D. S., Baxter, C. D. P., & Maretzki, S. (2009). A probabilistic approach for determining submarine landslide tsunami hazard along the upper east coast of the United States. *Marine Geology, 264*(1–2), 74–97.

Harbitz, C. B., Løvholt, F., & Bungum, H. (2014). Submarine landslide tsunamis: how extreme and how likely? *Natural Hazards, 72*(3), 1341–1374.

Harbitz, C. B., Løvholt, F., Pedersen, G., & Masson, D. G. (2006). Mechanisms of tsunami generation by submarine landslides: a short review. *Norwegian Journal of Geology, 86*(3), 255–264.

Imran, J., Parker, G., Locat, J., & Lee, H. (2001). 1D numerical model of muddy subaqueous and subaerial debris flows. *Journal of Hydraulic Engineering-Asce*, *127*(11), 959–968.

Kajiura, K. (1963). The leading wave of the tsunami: Bulletin of the Earthquake Research Institute Vol. 41, pp. 535–571.

Kawamura, K., Laberg, J. S., & Kanamatsu, T. (2014). Potential tsunamigenic submarine landslides in active margins. *Marine Geology, 356*, 44–49.

King, D. N., & Goff, J. R. (2010). Benefitting from differences in knowledge, practice and belief: Maori oral traditions and natural hazards science. *Natural Hazards and Earth System Sciences*, *10*(9), 1927–1940.

Lane, E. M., Gillibrand, P. A., Wang, X., & Power, W. (2013). A probabilistic tsunami hazard study of the Auckland Region, Part II: inundation modelling and hazard assessment. *Pure and Applied Geophysics*, *170*, 1635. doi:10.1007/s00024-012-0538-9.

Lane, E. M., Mountjoy, J. J., Power, W. L., & Popinet, S. (2016). Initialising landslide-generated tsunamis for probabilistic tsunami hazard assessment in Cook Strait. *The International Journal of Ocean and Climate Systems*, 4–13. doi:10.1177/1759313115623162.

Leonard, L. J., Rogers, G. C., & Mazzotti, S. (2014). Tsunami hazard assessment of Canada. *Natural Hazards, 70*(1), 237–274.

Lewis, K. B., Carter, L., & Davey, F. J. (1994). The opening of Cook Strait: interglacial tidal scour and aligning basins at a subduction to transform plate edge. *Marine Geology, 116*(3–4), 293–312.

Liu, P. L.-F., Wu, T.-R., Raichlen, F., Synolakis, C., & Borrero, J. C. (2005). Runup and rundown generated by three-dimensional sliding masses. *Journal of Fluid Mechanics, 536*, 107–144.

Løvholt, F., Lynett, P., & Pedersen, G. (2013). Simulating run-up on steep slopes with operational Boussinesq models; capabilities, spurious effects and instabilities. *Nonlinear Processes in Geophysics, 20*(3), 379–395.

Løvholt, F., Pedersen, G., Harbitz, C. B., Glimsdal, S., & Kim, J. (2015) On the characteristics of landslide tsunamis. *Philosophical Transactions of the Royal Society a-Mathematical Physical and Engineering Sciences*, *373*, 20140376. doi:10.1098/rsta.2014.0376.

Ma, G. F., Kirby, J. T., & Shi, F. Y. (2013). Numerical simulation of tsunami waves generated by deformable submarine landslides. *Ocean Modelling, 69*, 146–165.

Madsen, P. A., Bingham, H. B., & Schaffer, H. A. (2003). Boussinesq-type formulations for fully nonlinear and extremely

dispersive water waves: derivation and analysis. *Proceedings of the Royal Society a-Mathematical Physical and Engineering Sciences, 459*(2033), 1075–1104.

McFadgen, B. G., & Goff, J. R. (2007). Tsunamis in the New Zealand archaeological record. *Sedimentary Geology, 200*(3–4), 263–274.

Micallef, A., Mountjoy, J. J., Canals, M., & Lastras, G. (2012). Deep-seated bedrock landslides and submarine canyon evolution in an active tectonic margin: Cook Strait, New Zealand. In Y. Yamada, K. Kawamura, K. Ikehara, Y. Ogawa, R. Urgeles, D. Mosher, J. Chaytor, & M. Strasser (Eds.), *Submarine mass movements and their consequences* (Vol. 31, pp. 201–212). Netherlands: Springer.

Mountjoy, J. J., Barnes, P. M., & Pettinga, J. R. (2009). Morphostructure and evolution of submarine canyons across an active margin: Cook Strait sector of the Hikurangi Margin, New Zealand. *Marine Geology, 260*(1–4), 45–68.

Mountjoy, J. J., Micallef, A., Stevens, C. L., & Stirling, M. W. (2014). Holocene sedimentary activity in a non-terrestrially coupled submarine canyon: Cook Strait Canyon system. *New Zealand: Deep Sea Research Part II: Topical Studies in Oceanography, 104*, 120–133.

Mueller, C., Mountjoy, J. J., Power, W. L., Lane, E. M., & Wang, X. (2016) Towards a spatial probabilistic submarine landslide hazard model for submarine canyons. In G. Lamarche, J. Mountjoy, S. Bull, T. Hubble, S. Krastel, E. Lane, A. Micallef, L. Moscardelli, C. Mueller, I. Pecher & S. Woelz, (eds.) Submarine mass movements and their consequences, Vol. 41 (pp. 589–597). Springer, Berlin.

Okada, Y. (1985). Surface deformation due to shear and tensile faults in a half-space. *Bulletin of the Seismological Society of America, 75*(4), 1135–1154.

Okal, E. A. (2003). Normal mode energetics for far-field tsunamis generated by dislocations and landslides. *Pure and Applied Geophysics, 160*(10–11), 2189–2221.

Okal, E. A., & Synolakis, C. E. (2003). A theoretical comparison of tsunamis from dislocations and landslides. *Pure and Applied Geophysics, 160*(10–11), 2177–2188.

Okal, E. A., & Synolakis, C. E. (2004). Source discriminants for near-field tsunamis. *Geophysical Journal International*, *158*(3), 899–912.

Pampell-Manis, A., Horrillo, J., Shigihara, Y., & Parambath, L. (2016). Probabilistic assessment of landslide tsunami hazard for the northern Gulf of Mexico. *Journal of Geophysical Research-Oceans, 121*(1), 1009–1027.

Pedersen, G. (2008). Modeling runup with depth integrated equation models. In P. L. F. Liu, H. Yeh, C. Synolakis (Ed.), *Advanced Numerical Models for Simulating Tsunami Waves and Runup. Advances in Coastal and Ocean Engineering* (Vol. 10, pp. 3–41). Singapore: World Scientific.

Popinet, S. (2003). Gerris: a tree-based adaptive solver for the incompressible Euler equations in complex geometries. *Journal of Computational Physics, 190*(2), 572–600.

Popinet, S. (2011). Quadtree-adaptive tsunami modelling. *Ocean Dynamics, v*, *61*(9), 1261–1285.

Popinet, S. (2012). Adaptive modelling of long-distance wave propagation and fine-scale flooding during the Tohoku tsunami. *Natural Hazards and Earth System Sciences, v. 12*(4), 1213–1227.

Popinet, S., & Rickard, G. (2007). A tree-based solver for adaptive ocean modelling. *Ocean Modelling, 16*(3–4), 224–249.

Power, W. L. (2013). Review of Tsunami Hazard in New Zealand (2013 Update), GNS Science Consultancy Report 2013/131.

Proctor, R., & Carter, L. (1989). Tidal and sedimentary response to the late Quaternary closure and opening of Cook Strait, New Zealand: results from numerical modeling. *Paleoceanography, 4*(2), 167–180.

Savage, S. B., & Hutter, K. (1989). The motion of a finite mass of granular material down a rough incline. *Journal of Fluid Mechanics, 199*, 177–215.

Stirling, M., McVerry, G., Gerstenberger, M., Litchfield, N., Van Dissen, R., Berryman, K., et al. (2012). National seismic hazard model for New Zealand: 2010 Update. *Bulletin of the Seismological Society of America, 102*(4), 1514–1542.

Strasser, M., Koelling, M., Ferreira, C. d. S., Fink, H. G., Fujiwara, T., Henkel, S., Ikehara, K., Kanamatsu, T., Kawamura, K., Kodaira, S., Roemer, M., Wefer, G., SO219A, R. V. S. C., & scientists, J. C. M.-E. (2013). A slump in the trench: tracking the impact of the 2011 Tohoku-Oki earthquake, *Geology, v. 41*(8), 935–938.

Tappin, D. R., Grilli, S. T., Harris, J. C., Geller, R. J., Masterlark, T., Kirby, J. T., et al. (2014). Did a submarine landslide contribute to the 2011 Tohoku tsunami? *Marine Geology, 357*, 344–361.

Tappin, D. R., Watts, P., and Grilli, S. T. (2008). The Papua New Guinea tsunami of 17 July 1998: anatomy of a catastrophic event, *Natural Hazards and Earth System Sciences*, *8*(2), 243–266.

ten Brink, U. S., Chaytor, J. D., Geist, E. L., Brothers, D. S., and Andrews, B. D. (2014). Assessment of tsunami hazard to the US Atlantic margin. *Marine Geology*, *353*, 31–54.

ten Brink, U. S., Geist, E. L., & Andrews, B. D. (2006). Size distribution of submarine landslides and its implication to tsunami hazard in Puerto Rico. *Geophysical Research Letters*, *33*, L11307. doi:10.1029/2006GL026125.

ten Brink, U. S., Lee, H. J., Geist, E. L., & Twichell, D. (2009). Assessment of tsunami hazard to the US East Coast using relationships between submarine landslides and earthquakes. *Marine Geology, 264*(1–2), 65–73.

Voellmy, A. (1955). Über die Zerstörungskraft von Lawinen: Schweizerische Bauzeitung, *73*(12,15,17,19), 159–165, 212–217, 246–249, 280–285.

Walters, R. A., Gillibrand, P. A., Bell, R. G., & Lane, E. M. (2010). A study of tides and currents in Cook Strait, New Zealand. *Ocean Dynamics, 60*(6), 1559–1580.

Watts, P., Grilli, S. T., Kirby, J. T., Fryer, G. J., & Tappin, D. R. (2003). Landslide tsunami case studies using a Boussinesq model and a fully nonlinear tsunami generation model. *Natural Hazards and Earth System Sciences, 3*(5), 391–402.

Watts, P., Grilli, S. T., Tappin, D. R., & Fryer, G. J. (2005). Tsunami generation by submarine mass failure. II: predictive equations and case studies. *Journal of Waterway Port Coastal and Ocean Engineering-ASCE. 131*(6), 298–310. doi:10.1061/(ASCE)0733-950X(2005)131:6(298).

WREMO (2015). Tsunami evacuation zone maps. Wellington Region Emergency Management Office. http://www.getprepared.org.nz/tsunami-zone-maps. Accessed 28 Apr 2016.

(Received April 30, 2016, revised September 28, 2016, accepted September 29, 2016, Published online October 14, 2016)